Thermodynamic anomalies near the critical point of CO_2 †

John A. White and Bruce S. Maccabee*
The American University, Washington, D. C.
(Received 12 August 1974)

Existing experimental data on the compressibility, chemical potential, specific heat, and critical opalescence of CO_2 are analyzed to determine a parametric, scaling-law representation for the critical region. A representation of the form of the linear model of Schofield is found to be consistent with these data for scaling-law amplitudes $a = 22$, $b^2 = g = 1.30$, exponents $\beta = 0.347$, $\gamma = 1.22$, $\alpha = 0.09$, and for a slowly varying (nondivergent) background. This representation corresponds approximately to the use of the mean range of local density correlations and of the macroscopic order as fundamental (parametric) variables to locate positions in thermodynamic space. The representation thus obtained is used to predict effects of gravity and the shape of contours of equal wave scattering close to the critical point. The predictions are investigated experimentally by studying the dependence of the scattering of laser light on chemical potential (height) and temperature. Satisfactory agreement is found to within the precision of the measurements. In addition, it is verified experimentally that contours of equal opalescence have the same shape as contours of equal mean relaxation time of local density fluctuations. This demonstrates that the relaxation time and the correlation length obey equivalent scaling-law homogeneity relationships close to the critical point. Some discrepancies among existing experiments and between experiment and theory are noted and discussed briefly. In particular, there remain unexplained discrepancies between the values of the critical-point exponents found here and those predicted by the Ising model.

I. INTRODUCTION

A. Background

As the temperature of a simple fluid is increased, the crisp distinctions of macroscopic phase that separate gas from liquid at low temperatures fade until, at the critical point and at higher temperatures, the fluid no longer exhibits a discontinuous change of phase with change of pressure. It can then no longer be characterized unambiguously as either liquid or gas.

In the vicinity of the critical point, new features become prominent. On a macroscopic level, these include critical opalescence and anomalies (divergences) of the compressibility, specific heat, thermal conductivity, and diffusivity. Microscopically, fluctuations become an increasingly dominant feature. Local deviations from average density (fluctuations) are always present, fleetingly, within each phase, as a result of thermal agitation. However, as a critical point is approached the correlations among local deviations at different points in a fluid increase appreciably both in spatial extent and temporal duration. In effect, each phase develops bubbles of above and below average density. These "bubbles," of irregular shape and diffuse boundaries, increase substantially in size and decrease markedly in mobility as the critical point is approached. The growth of these locally correlated deviations is responsible for anomalous static and transport properties in the vicinity of critical points.

To best represent the thermodynamic properties of a fluid in the vicinity of its critical point, an equation of state should be based upon, or at least compatible with, the anomalous properties which arise from the growth in spatial extent of the locally correlated deviations. Such an equation of state could be one in which the macroscopic thermodynamic variables (density, temperature, chemical potential, etc.) are expressed in terms of one parameter which characterizes the locally correlated deviations from average order and another which characterizes the average order for a given value of the first parameter. It is known that important quantitative features of the thermodynamic anomalies (the strengths of the divergences) are related to a single quantity that characterizes the localized deviations from average density (a specific type of order). This quantity is the mean *range of cooperation (correlation length)* of these deviations, or the mean "bubble" radius. The magnitude of the compressibility anomaly and the strength and anisotropy of scattering responsible for critical opalescence[1] have been related to this range,[2,3] as has also the strength of the divergence of the thermal diffusivity.[4] If a thermodynamic variable that is closely related to the correlation length of density deviations is chosen as one of the above parameters, then the other parameter should be closely related to the average density.

To incorporate these parameters into an equation of state for the fluid, it is necessary to make use of a transformation from conventionally measured parameters, such as temperature, pres-

sure, and density, to new variables which are related to the correlation range and the average density. It will be convenient for this purpose to employ a parametric representation.[5,6] A pair of parametric variables, r and θ, will be defined as functions of temperature T and density ρ. They will be chosen so that r (the "remoteness" from the critical point) is closely related to the correlation range of the fluctuations (increasing as that range decreases) and θ ("order parameter") is an increasing function of the average density at constant r that defines the macroscopic phase of the fluid. Together θ and r suffice in place of ρ and T to specify any equilibrium thermodynamic state.

Several parametric models have been proposed,[7-9] the simplest of which is known as the (unrestricted) linear model.[6,7] In this work we have compared the predictions of this model with CO_2 thermodynamic and light-scattering data. However, in doing so, we have imposed a new requirement on the model. We have required that the parameter r be as nearly as possible a simple (exponential) function of the susceptibility, $\chi = (\rho^2 K_T)$, because this susceptibility is closely related to the density-fluctuation correlation range[2,3] in the immediate vicinity of the critical point where the linear model is expected to be applicable. The consequences of this requirement are as follows: (i) The constant known as b^2 in the model is smaller than the value proposed by Schofield, Litster, and Ho (SLH)[7]; (ii) as a result of (i) the model has a "true" spinodal behavior in that the compressibility diverges along a curve that lies inside the coexistence curve; (iii) susceptibility and chemical-potential data in the vicinity of the critical point are well represented by the model; and (iv) the available specific-heat data can also be well represented by the model. Thus, by using PVT data, specific-heat data, light-scattering data that are found in the literature, and light-scattering data that are presented here for the first time, we have been able to adjust the constants in the linear-model equation so that it represents the available data to within about a 5% accuracy. We believe that this is the first time such good over-all agreement with critical-point data has been achieved.

A detailed plan of this paper and summary of our principal new results is presented in the following synopsis.

B. Synopsis

In the first of the sections to follow (Sec. II) bulk measurements of pressure, volume, and temperature[10] are analyzed to determine contours of constant susceptibility.[11] These contours, together with the coexistence curve[12] and the requirement we impose—that contours of constant susceptibility approximate contours of constant r—suffice to determine three of Schofield's linear-model parameters,[6] b^2, g, and β, to two significant figures. Agreement for this choice of parameters with some of the experimental data is exhibited in Table I. Reasons are stated for the small discrepancies apparent in this table. In Appendix C it is shown in detail how the data discussed thus far (susceptibility contours and coexistence curve) lead naturally to the particular linear-model parametric equations of state (summarized in Appendix B) that are used in the rest of this investigation.

Next, in Sec. III, the temperature dependence of the compressibility at critical density, as derived from PVT[10] and light-scattering data,[13,14] is used to determine independently of b^2 and β accurate numerical values of the remaining two model parameters, a and γ. Reasons are presented to explain differences between previously proposed values for γ. The value of a, which is the least precisely determined of the model parameters, is found to be constrained by the compressibility data to be a certain (empirical) function of two of the other parameters, g and γ. The linear-model parameters determined thus far give a predicted ratio of susceptibilities above and below T_c that agrees with experiment.[13]

Numerical values for the linear-model parameters found in other recent investigations[15,16] are noted. They differ considerably among themselves and some of them differ considerably from those obtained here. Some reasons for the discrepancies are stated.

The work to this point, described in Secs. II and III, leads to a complete specification of the thermodynamics of CO_2 in a linear-model approximation. The adequacy of this model is tested in the following sections by comparing in detail predictions of the model (Appendix B) with several different types of experimental data.

First, in Sec. IV, a more detailed comparison is made with the PVT data.[10] The model permits susceptibilities[10] and chemical potentials[17] derived from pressure measurements to be normalized to two universal curves (Figs. 4 and 5). Agreement with model predictions is to within the experimental uncertainty of ~5% for $r < 0.03$ and $|\theta| < 0.8$. For larger values of r and θ, the breakdown of perfect scaling-law symmetries becomes appreciable. Reasons for the departures from perfect symmetry are discussed. It is noted that no error outside experimental uncertainties is made for any θ for our choice of linear-model parameters, including especially our choice for b^2, for small r. (A model equation of state that incorporates cor-

rection terms[18] to describe the asymmetries at larger r has been fitted to the CO_2 susceptibility data and been found to work out to $r=0.3$ and $\theta = \pm 1.0$.[19])

Model predictions are compared with specific-heat data[20] in Sec. V. The comparison leads to a further refinement of the model parameters. To make this refinement, it is necessary to assume that the exponent α that describes the divergence of the specific heat is smaller than the value 0.125 originally found[20] to fit the specific-heat data. It is noted (Appendix D) that values as small as 0.08 can result in a fit to the measured specific heat to within ~1%. Using $\alpha=0.09$, we find an excellent fit to both branches of the specific-heat curve (above and below T_c) for choices of the other parameters of the model compatible with the PVT and light-scattering data, and compatible with our restriction on the choice of b^2. For our best fits, the background contributions to the specific heat are the same above and below T_c. Our best fits, however, leave a discrepancy ~2% very close to T_c that cannot be removed by further small adjustments in the values of the parameters.

A final choice of model parameters is made and exhibited in Sec. V (Table III). The values for the parameters stated there are compared with values proposed for the same parameters in other recent investigations.[15,16] The parameter values found in the present investigation give an order of magnitude improvement in the fit to the specific-heat data, and in particular to the ratio of specific heats measured above and below T_c. Agreement over-all, with specific-heat, PVT, and light-scattering data, is good enough (~3% with much of the most accurate data) to justify a confidence that the model gives an essentially correct description of all critical-point phenomena, at least when r is sufficiently large to assure that the compression of the fluid under its own weight is of secondary importance. In the sections that follow, the model thus specified is used closer to the critical point (for $r<10^{-4}$) to interpret experiments performed to study effects of this compression.

The variation of density with vertical position in the fluid is considered in Sec. VI. Height profiles predicted by the model equations for isothermal conditions are compared with profiles determined by Schmidt and Straub[21,22] from measurements of the refractive index of CO_2 as a function of height. There is serious disagreement, amounting to a factor-of-3 discrepancy in the "best-fit" value to use for the model parameter a. A detailed consideration (Appendix F) shows that the discrepancy can be explained by the presence of a thermal gradient in the experiments of ~0.6 mdeg/cm (top of the cell warmer than the bottom). A thermal gradient of this magnitude seems to have been within the thermal tolerances of the experiments.

In Secs. VII and VIII we turn to the analysis of some light-scattering measurements performed very close to the critical point and reported here for the first time. These measurements have been performed in a region ($r \lesssim 10^{-4}$) where effects of the compression of a fluid under its own weight are prominent.

In Sec. VII we consider the variation of the susceptibility of the fluid at equilibrium with temperature and vertical position. The variation of the susceptibility predicted by the model equations is compared with the results of light-scattering measurements.[23] The intensity of scattering is expected to be proportional to the susceptibility[1,2] for infinitely thin samples. However, for the 0.5-cm-thick samples used in the experiments, extinction is large,[13] with the result that measured intensity-height profiles uncorrected for extinction differ appreciably from predicted susceptibility profiles (Fig. 6).

In Sec. VIII, a novel method[23] for making light-scattering measurements close to the critical point is described. In this method the temperature and vertical position within the fluid are both changed to map a contour of constant scattered intensity. The shape of this contour is largely insensitive to effects of extinction and tests directly the shape of the underlying thermodynamic surface without the need to make corrections for extinction. The shapes of predicted and observed contours are compared (Fig. 8), and agreement is found to be good, to within the ~10% accuracy of existing measurements.[23] Thus, no evidence is found to this accuracy for a breakdown of the model or of a need to use different parameter values very close to the critical point.

Additional data are presented in Sec. VIII on the *spectrum* of the scattered light. The inverse of the width of the spectrum is proportional to the mean time for growth and decay of the spontaneous fluctuations of density within the fluid, and hence is a measure of a transport property (diffusivity) of the fluid. Contours of constant spectrum (constant relaxation time) have been mapped and found to be of the same shape as contours of constant scattered intensity. Thus, to within the accuracy of the measurements reported here, contours of constant transport phenomena (diffusivity) coincide with contours of constant static properties (susceptibility). These measurements, performed close to the critical point ($r \lesssim 10^{-4}$), contribute to confidence that a single critical-point scaling-law theory, approximated for CO_2 by the model equations and choice of b^2 employed in this investiga-

tion, correctly describes the cooperative phenomena responsible for all anomalies, dynamic and static, present in the vicinity of a critical point.

A summary of the principal general conclusions of this investigation is presented in Sec. IX.

II. COEXISTENCE CURVE AND SUSCEPTIBILITY CONTOURS

Extensive and accurate PVT measurements made several decades ago[10] establish that the thermodynamic surface of CO_2 has the general shape shown in Fig. 1. Of particular interest are the isoclines of that surface, which define contours of constant susceptibility (see the summary of definitions given in Appendix A). These contours when viewed in the T,ρ plane [Fig. 1(b)] have the form of a family of inverted parabolas. Experimentally determined contours are shown in Fig. 2.[11] The data in that figure cover a rather wide range of temperature (10–140°C) and density (60–460 amagat) in the single-phase region around the critical point ($T_c = 31$°C, $\rho_c = 237$ amagat). The data cover a large enough range to show departures from perfect symmetry at substantial distances from the critical point.

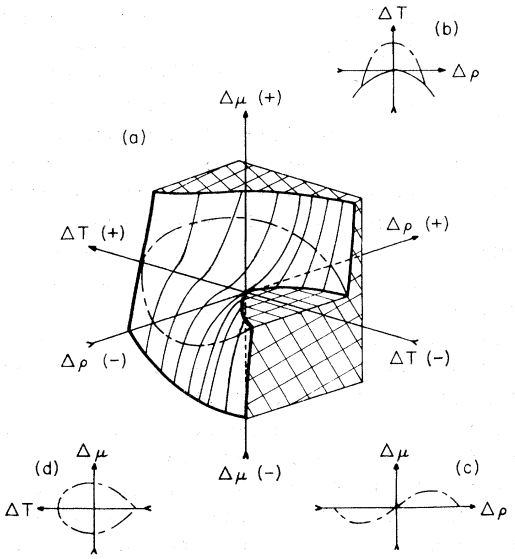

FIG. 1. Thermodynamic surface in the vicinity of the critical point. (a) The real (physical) surface is bounded by the heavy line. This line consists of contours of constant ΔT and contours of constant $\Delta\mu = \mu(\rho, T) - \mu(\rho_c, T)$. The coexistence curve lies in the T-ρ plane. The cross-hatched regions lie "below" the surface. The lines which lie in and illustrate the curvature of the surface are isotherms. The short-long dashed line is an "isocline"—a line of constant slope, $(\partial\mu/\partial\rho)_T$. (b) The constant $(\partial\mu/\partial\rho)_T$ line projected onto the T-ρ plane. (c) The same isocline viewed along the temperature axis. (d) The isocline viewed along the density axis. The critical point is at the origin of each figure; the figures are not drawn to scale.

Significant features of the susceptibility data of Fig. 2 close to the critical point are described most simply in terms of parametric variables, illustrated in Fig. 3. An approximate representation of these features is given by contours of constant r and constant θ in the linear-model parametric representation of Schofield,[6] illustrated in Fig. 3(b) for particular choices of the parameters of the model. The equations of the contours shown in Fig. 3(b) are

$$\Delta\rho = g\rho_c r^\beta \theta, \tag{1a}$$

$$\Delta T = T_c r(1 - b^2\theta^2). \tag{1b}$$

Here ρ_c and T_c are, respectively, the density and temperature at the critical point, $\Delta\rho = \rho - \rho_c$, $\Delta T = T - T_c$, and g, β, and b^2 are three dimensionless constants, with $b^2 > 1$. The dimensionless constants determine the shape of the coexistence curve ($\theta = \pm 1$),

$$\Delta\rho = \pm g\rho_c[(1 - b^2)^{-1}\Delta T/T_c]^\beta, \tag{2}$$

and the relation at constant r,

$$\Delta\rho(T = T_c) = \pm g\rho_c b^{-1}[\Delta T(\rho = \rho_c)T_c^{-1}]^\beta, \tag{3}$$

which connects the densities at the critical temperature with the temperature at the critical density for the same r.

The dimensionless constants may be adjusted so that (i) the $\theta = \pm 1$ curves [Eq. (2)] approximate the two branches of the experimental coexistence curve and (ii) the $T = T_c$ and $\rho = \rho_c$ intercepts of contours of constant r [Eq. (3)] occur at approxi-

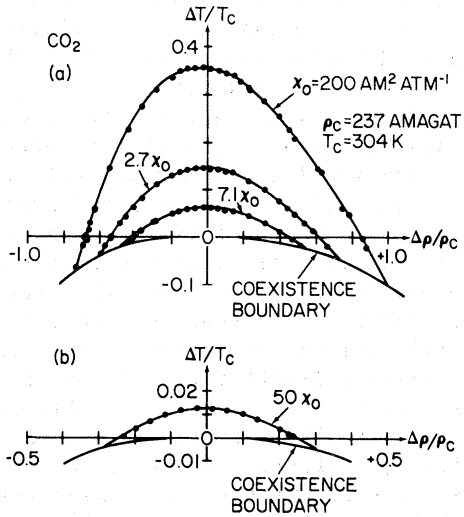

FIG. 2. Contours of constant susceptibility in CO_2. Data are from Ref. 10. The solid lines are empirically determined fits to the data (Refs. 11, 19). Note the expanded scales used in Fig. 2(b).

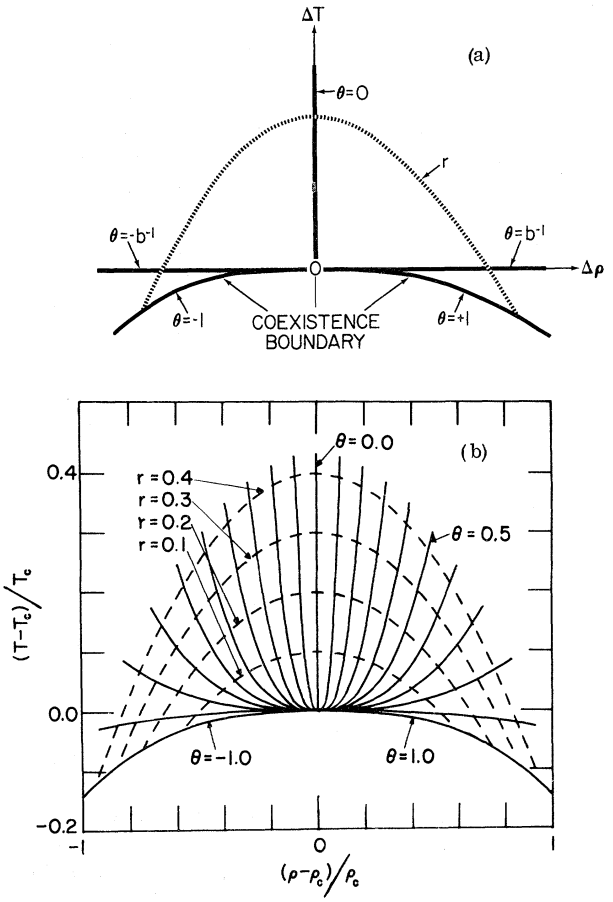

FIG. 3. (a) Contours of constant θ (solid lines) and constant r (dashed line) in the T-ρ plane. The critical point is at $r=0$. (b) The form of these contours given by Eq. (1) when $\beta=0.35$ and $g=b^2=1.3$.

mately the same locations as the corresponding intercepts of constant susceptibility (or constant correlation length). An analysis of the coexistence curve of CO_2 (Ref. 12) and of contours of constant susceptibility[10,11,24] indicates that requirements (i) and (ii) lead to $\beta \simeq 0.347$ with $T_c \simeq 31.00°C$, $g(b^2-1)^{-\beta} \simeq 1.96$, $g/b \simeq 1.12$, where in each case the last significant figure is uncertain by $\simeq \pm 3$. (The critical density is about 236.8 ± 0.1 amagat $=0.468$ g/cm^3.) This results in the following set of values for β, g, b^2:

$$\beta = 0.35, \tag{4a}$$

$$g = b^2 = 1.3. \tag{4b}$$

The constants (4) have been rounded off to two significant figures for use as a first approximation consistent with and within the error bars of the measurements of (2) and (3).

The prediction (3) for this choice of constants is compared with susceptibilities measured over a wide range of temperature and pressure in Table I. Agreement over-all tends to be within ~3% when experimental intercepts at $\Delta\rho \gtrless 0$ are averaged, with somewhat better agreement for the $\Delta\rho > 0$ branch than for the $\Delta\rho < 0$ branch.

The discrepancy between real and calculated quantities in Table I results partly from errors in choosing the constants (4) and partly from the fact that contours of constant r in the linear model (see Fig. 3) and contours of constant susceptibility that have been constructed from the experimental data[11,19,24,25] (see Fig. 2) do not exactly coincide at the critical isotherm, $\theta = 1/b$, as well as at the critical isochore, $\theta = 0$. However, the major discrepancy between the real and calculated values in Table I results from the fact that the fluid is inherently asymmetric about the critical density,[17,19] with the asymmetry increasing as $|\Delta T|$ increases (see Fig. 2), while the linear model is "everywhere" symmetric. A quantitative approach to the representation of this asymmetry is presented elsewhere.[11,19,25] For the purposes of this paper it is sufficient to point out that as the critical point is approached the asymmetry becomes less and less evident, so that, within some empirical boundary, the fluid data may be represented quite accurately by a totally symmetric equation of state. (For CO_2 this boundary is roughly a contour of constant r with[19] $r \sim 0.01$.)

III. COMPRESSIBILITY AS A FUNCTION OF TEMPERATURE

The exponent γ can be estimated independently of g, b^2, and β by considering the dependence of the susceptibility on temperature along the critical isochore ($\rho = \rho_c$, $\theta = 0$). Measurements made over a wide range of $\Delta T > 0$ have given results[13,14] which

TABLE I. Maximum temperature, $T_p - T_c$, with $T_c = 31.00$ °C, and intercepts on the critical isotherm of contours of constant susceptibility (Fig. 2): (a) experimental results, Ref. 10; (b) intercepts predicted by Eqs. (3) and (4). The experimental values for $\Delta\rho$ are uncertain to ~ 1% of $\Delta\rho$.

	(a) Experiment		(b) Theory
χ (10^2 amagat^2 atm^{-1})	$T_p - T_c$ (°C)	$\Delta\rho(T=T_c)$ (amagat)	$\Delta\rho(T=T_c)$ (amagat)
100	3.83	−56, +58	±58.5
50	6.67	−67, +73	±71.0
25	11.8	−83, +88	±86.6
14	19.1	−97, +106	±102.4
10	26.1	−107, +120	±114.3
5.4	44.1	−126, +144	±137.3
3.3	68.6	−142, +169	±160.3
2.0	109	−161, +191	±187.8

are comprised in the statement

$$K_T^{-1} = 16(0.01)^{1.2-\gamma} P_c (\Delta T/T_c)^{\gamma}, \tag{5}$$

with[13] $\gamma \simeq 1.17$ or[14] $\gamma \simeq 1.219$. The different values of γ reflect differences of interpretation of light-scattering data, experimental uncertainties, and a difference in weights attached to data obtained at the extremes of the temperature range. In particular, the lower exponent gives better agreement with data obtained far from T_c (Table I) and the higher exponent better agreement close to T_c. (The light-scattering data of Ref. 13 are compatible with a value of the compressibility exponent that varies from $\gamma \gtrsim 1.20$ for small ΔT to $\gamma \lesssim 1.17$ for large ΔT.)

The approximations

$$\gamma = 1.2, \tag{6a}$$

$$a = 21 \tag{6b}$$

are consistent with the choice (4) and the relations (A7), (E1), (B6), and (5). (Equations whose numbers are preceded by a letter are found in the Appendix of the same letter.) More generally, for different choices of γ, the constant a is constrained by (B6) and (5) to have the value

$$a = 16g(0.01)^{1.2-\gamma}. \tag{7}$$

In the model critical state (B1), the susceptibility (B6) is smaller than (5) for $\Delta T < 0$ and $\theta = \pm 1$ by a factor $\chi_+/\chi_- = 2(b^2-1)^{1-\gamma}[1 - b^2(1-2\beta)]^{-1}$ that becomes ≈ 4.17 for the choices (4), (6a). The experimentally determined factor is[13] $\chi_+/\chi_- \approx 4.0$, with an uncertainty ~0.3. The experimental uncertainty of (5) at $\Delta T/T_c = 0.01$, and hence the uncertainty of the numerical coefficient in (7), is approximately 5%.

A choice $\gamma = 1.2$ and $a = 20$, to be employed in some of the discussion to follow, is compatible with (7) within its error bar. This choice of constants provides a somewhat better average fit to (5) than does (6) in the case that the empirical relation (5) actually should be used with γ varying from $\gamma > 1.2$ for small $|\Delta T|$ to $\gamma < 1.2$ for large $|\Delta T|$. The choice $\gamma = 1.20$ is then an average value and the choice $a = 20$ is a best-fit value for use when the value $\gamma = 1.20$ is used over the whole temperature range.

It may be noted that the choice $\gamma = 1.2$, $a = 20$, and the choice of constants given by (4) agrees to within 6% with the corresponding parameters ($\beta = 0.3486$, $b^2 = 1.35$, $g = 1.37$, $a = 19.6$, $\gamma = 1.178$) found by Murphy, Sengers, and Sengers[16] in a fit to Michels's pressure, density, and temperature data[10] on CO_2 using the "restricted" linear model. There is substantial disagreement, however, with their unrestricted linear-model results ($\beta = 0.3486$, $b^2 = 1.70$, $g = 1.75$, $a = 24.48$, $\gamma = 1.175$) which they found to give better agreement with the same pressure data. It is to be noted that their result $b^2 = 1.70$ for this latter model is incompatible with an interpretation that contours of constant r should closely approximate contours of constant susceptibility (or constant correlation length). For this reason, and others mentioned in Appendix BD and in Sec. V, we prefer to employ an unrestricted linear model with a smaller value of b^2. The "restricted" model parameters $\beta = 0.347$, $b^2 = 1.44$, $g = 1.49$, $a = 28.37$, $\gamma = 1.24$ obtained by Hohenberg and Barmatz[15] differ more from our own than the more recent restricted model set of parameters found by Murphy *et al.*[16]

IV. SUSCEPTIBILITY AND CHEMICAL POTENTIAL AS FUNCTIONS OF DENSITY AND TEMPERATURE

A detailed comparison of the predictions (B1c) and (B6) with the choice of constants $\beta = 0.35$, $g = b^2 = 1.3$, $a = 20$, $\gamma = 1.20$ and experimental data derived from bulk measurements of pressure, volume, and temperature[10] is presented in Figs. 4 and 5.

Agreement with the average observed chemical potential[17] (Fig. 4) is to within ≃3%. (Individual data points have an rms deviation ≃5%.) The data correspond to values of r in the range $0.0007 < r < 0.03$, for which there is almost perfect antisymmetry about $\Delta\rho = 0$ ($\theta = 0$). Scatter in the data is greatest for $r < 0.003$, where the experimental uncertainties in ΔT, $\Delta\rho$, $\Delta\mu$ are greatest.

The inverse susceptibilities plotted in Fig. 5 encompass a wider domain of $\Delta\rho$ and ΔT (corre-

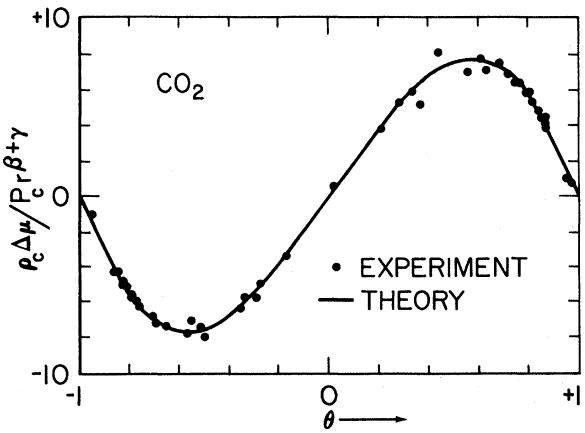

FIG. 4. Dependence of the chemical potential on θ (density) at constant r. Data are from Ref. 17, plotted for $T_c = 31.00\,^{\circ}C$. The solid curve corresponds to Eq. (B1c).

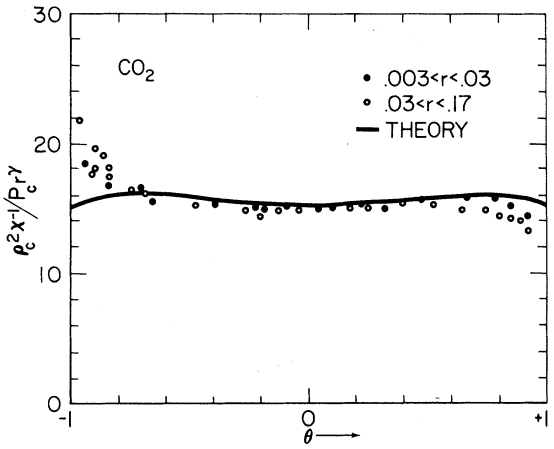

FIG. 5. Susceptibility as a function of θ and r. Data are from Ref. 10, plotted for $T_c = 31.00\,^\circ$C. The solid line is given by Eq. (B6).

sponding to $r \leq 0.17$) and show convergence toward linear-model behavior [Eq. (B6)], which is represented by the solid line, as r decreases. For the restricted range $r < 0.03$ used in Fig. 4, the susceptibility remains constant to approximately 5% along most of a contour of constant r. The rather good agreement between the predictions of the simple (linear) parametric model and the susceptibility data is not unexpected, because a careful study of these data by themselves[11] has led us to conclude that a parametric equation is a "natural" equation for the representation of such data (see Appendix C).

Appreciable deviations from constancy and from (B6) are confined primarily to larger values of r and the regions $|\theta| > 0.8$, for which $|\Delta\rho|$ is large. The largest deviations, for $\theta < -0.8$, reflect the presence of the absolute boundary at $\Delta\rho_{\min} = -\rho_c$ (rarified gas) at which $\chi^{-1} \to \infty$. The behavior of the susceptibility near this boundary is expressed most naturally in terms of ρ, T rather than r, θ coordinates; the divergence of χ^{-1} in this region of dilute gas corresponds to a component of $(\chi^{-1})_b$ in (E1) proportional to ρ^{-1}. The deviations from the prediction (B6) for large r and $\theta > +0.8$ may correspond to a background $(\chi^{-1})_b$ that continues to be dependent on ρ when ρ is large.

Additional deviations for small r and $|\theta| \approx 1$ can be expected if the anomalous behavior near $|\theta| = |\theta_m|$ and its extreme sensitivity to the choice of value for b^2 (cf. the discussion in Appendix B D) are indicative of a defect of the model equation of state or choice of b^2 that we have used. Any such additional deviations for small r seem at present, however, to fall within the limits of accuracy of existing data.

For the same choices of b^2, β, and g, provided the constraint (7) is satisfied, other choices of γ in the range $\gamma = 1.20 \pm 0.03$ yield results similar to those shown in Figs. 4 and 5.

V. SPECIFIC HEAT

The experimental dependence on temperature of the specific heat of CO_2 is[20]

$$\frac{C_V}{R} = A_\pm \left| \frac{\Delta T}{T_c} \right|^{-\alpha_\pm} + B_\pm , \tag{8}$$

where R is the gas constant and $A_+ = 5.583$, $A_- = 10.473$, $B_+ = -3.457$, $B_- = -0.024$, $\alpha_+ = \alpha_- = 0.125$. (The subscripts plus and minus refer to temperatures, respectively, above and below T_c.)

The experimentally determined ratio

$$A_-/A_+ = 1.876 \tag{9}$$

may be compared with that predicted for the model critical state [Eqs. (B5) for $\theta = 0$ and (B9)]:

$$\frac{A_-}{A_+} = \frac{f_0 + f_2 + f_4}{(b^2 - 1)^{\gamma + 2\beta} f_0} . \tag{10}$$

For $b^2 = 1.30$, $\beta = 0.35$, the theoretical ratio is

$$A_-/A_+ = 2.07 \quad \text{for } \gamma = 1.20, \tag{11a}$$

$$A_-/A_+ = 1.76 \quad \text{for } \gamma = 1.22. \tag{11b}$$

The predictions (11) are sensitive to β (rather insensitive to b^2). The choice

$$\gamma = 1.217, \quad \beta = 0.347, \quad g = b^2 = 1.30, \tag{12}$$

which gives $A_-/A_+ = 1.86$, is compatible with the experimental ratio (9) and also with the shape of the coexistence curve (Sec. II). Significantly poorer agreement with the experimental ratio of specific heats is obtained using either the parameters of the restricted linear model or those of the unrestricted linear model employed by Murphy *et al.*[16] Using the parameters quoted by Murphy *et al.*, the theoretical ratio (10) becomes $A_-/A_+ = 2.54$ (restricted model) or 2.98 (unrestricted model). The theoretical value for the ratio obtained by using the restricted-linear-model parameters of Hohenberg and Barmatz[15] is $A_-/A_+ = 1.53$. Use of our parameter values $\gamma = 1.217$ and $\beta = 0.347$ in the Ho-Litster[9] (cubic) model (cf. end of Appendix C) leads to values of $b^2 = b^2_{\text{HL}} = 3/(3 - 2\beta)$ and of the specific-heat ratio[25] almost identical to the values (12) and (9), as found above using our version of the unrestricted linear model.

Above T_c along the critical isochore ($\theta = 0$) the specific heat (B5) is

$$(c_\rho)_a = \frac{-agP_c c_0 T}{T_c^2} \left(\frac{\Delta T}{T_c} \right)^{\gamma + 2\beta - 2} . \tag{13}$$

This expression cannot exactly reproduce the temperature dependence stated in (8) when $2 - \gamma$

$-2\beta = \alpha \neq 0.125$. However, as discussed in Appendix D, for values of α not too far different from 0.125 there is good numerical agreement for suitable choices of a and g. For example, for $g = 1.30$ and $\beta = 0.35$, agreement of (13) with the temperature-dependent part of (8) *above* T_c is to within ~1% over most of the range of temperatures for which reliable data are available for the choices

$$\gamma = 1.20, \quad \alpha = 0.10, \quad a = 23.4, \tag{14a}$$

or

$$\gamma = 1.22, \quad \alpha = 0.08, \quad a = 23.9. \tag{14b}$$

Agreement with Eqs. (B9) and (B8) *below* T_c to ~1% is obtained for the same choices of γ and α for somewhat different values of a. Table II summarizes values of $a_\pm$ and added background $B_\pm$ that, used with Eqs. (13) and (B9), fit the specific-heat data (8) above (+) and below (−) T_c to ~1% for the choices of exponents discussed above. In the same table are listed the values of a required to fit the susceptibility [(B6a), (7)] for the same choices of exponents.

When the scaling-law requirement that B_+ and B_- be equal[17] is applied for $\beta = 0.35$, $g = b^2 = 1.3$, $\gamma = 1.20$, $a = 20$, and $B_+ = B_- = -7$ there is over-all agreement with *both branches* of the specific heat and with the compressibility (7) to better than 10%. Over-all agreement improves for each of the following modifications: (a) slightly smaller β, (b) somewhat larger γ compatible with (7). As an example, the choices $g = b^2 = 1.30$, $\beta = 0.347$, $\gamma = 1.217$, $a = 22$ [Eqs. (7), (12)] used with equal background contributions $B_+ = B_- = -8.9$ lead to agreement with all of the specific-heat data[20] and the compressibility to $\lesssim 3\%$.

Agreement with the specific heat in the range $10^{-4} < |(T - T_c)/T_c| < 10^{-2}$ measured both above and below T_c can be improved to ~1% without noticeably changing the agreement with the compressibility with further small modifications of the values of the parameters used in the equations. Examples of such modifications that lead to improved agreement with (8) for the same choice of background ($B_\pm = -8.9$) include use of $\beta = 0.346$, $\alpha = 0.087$, $b^2 = 1.31$; use of $\beta = 0.344$, $\alpha = 0.089$, and either $g = 1.28$ or $b^2 = 1.31$; or use of $\beta = 0.342$, $\alpha = 0.090$, $g = 1.28$, $b^2 = 1.31$, $a = 22.2$. There remains a small possibly significant discrepancy with (8), especially for small $|\Delta T|$. The discrepancy grows to >2% for $(T - T_c)/T_c = \pm 4 \times 10^{-5}$, the smallest ΔT studied experimentally. This discrepancy cannot be removed by making additional small changes in the values of the parameters. Further consideration of this point, which will not be undertaken here, as well as efforts to improve significantly on the values of the parameters cited in the previous paragraph, should take into consideration effects of compression of fluids under their own weight and the lengthening of thermal equilibration times that occurs close to the critical point. Consideration might also have to be given to the possible effect on the numerical values of these parameters caused by contamination or whatever other factor accounts for the difference between the values of T_c found in most of the experiments discussed (31.0°C) and that obtained in the calorimetric measurements (30.8°C).[20]

This completes our analysis of experimental data to obtain a set of constants to use in the unrestricted-linear-model equations of the critical state. The more refined of the two sets of parameters with $g = b^2 = 1.30$ discussed above (that accurate to ~3%) is listed in Table III together with values for these parameters obtained in other recent investigations.

The constants used in the model equation of state have been determined above from experiments performed sufficiently far from the critical point that the compression of a fluid under its own weight is of secondary importance. In the following sections the model thus specified will be used to interpret experiments performed to study effects of this compression. The results of these experiments will be examined to see if they verify the theory for regions of thermodynamic space that are too close to the critical point to be studied effectively by the types of investigations considered to this point.

VI. DENSITY AS A FUNCTION OF HEIGHT

According to (F2), (E2), and (B1), the density of a linear model fluid at constant temperature

TABLE II. Values of a and B required to fit the measured compressibility [Eq. (7)] and specific heat [Eqs. (8), (B9), and (13)] for $g = b^2 = 1.30$ and different choices of critical exponents. Subscripts plus and minus refer to temperatures, respectively, above and below T_c.

Exponents			Compressibility	Specific heat			
α	β	γ	a_+	a_+	a_-	B_+	B_-
0.10	0.35	1.20	21	23.4	21.2	−7.1	−7.0
0.08	0.35	1.22	23	23.9	25.5	−11.8	−15.6
0.089	0.347	1.217	22.7	22.9	23.2	−9.4	−11.4

TABLE III. Parameters for use with the "linear-model" representation of the critical region of CO_2. Columns marked with an asterisk correspond to the "restricted" model, for which b^2 is constrained to satisfy Eq. (B10).

Source	Hohenberg and Barmatz*[a]	Murphy *et al.*[b]	Murphy *et al.*[b]	Present investigation
α	0.065	0.13	0.13	0.089
β	0.347	0.3486	0.3486	0.347
γ	1.241	1.178	1.175	1.217
a	28.4	19.6	24.5	22.0
b^2	1.44	1.35	1.70	1.30
g	1.49	1.37	1.75	1.30

[a]Reference 15. [b]Reference 16.

varies with height in accordance with the parametric relation

$$\Delta z = a z_0 r^{\gamma+\beta}(\theta - \theta^3), \tag{15}$$

with

$$-z_0 = P_c(m\rho_c g_0)^{-1}. \tag{16}$$

Here Δz is the distance above that elevation $z(\rho_c)$ in the fluid at which $\rho = \rho_c$. It follows from (B1) and (15) that for $T > T_c$ and small $\Delta\rho$

$$\Delta z = \frac{z_0 a \Delta\rho}{g\rho_c}\left(\frac{\Delta T}{T_c}\right)^{\gamma}, \tag{17a}$$

and for $T = T_c$, $\Delta\rho \neq 0$,

$$\Delta z = \frac{z_0 a b^{\delta-3}(b^2-1)\Delta\rho}{g^{\delta}\rho_c}\left|\frac{\Delta\rho}{\rho_c}\right|^{\delta-1}, \tag{17b}$$

where $\delta = (\gamma/\beta)+1$.

The predictions (17) are in qualitative agreement with density profiles measured in CO_2 by Schmidt and Straub.[21,22] Quantitatively, however, the value of a required to fit Schmidt and Straub's data is much smaller (by about a factor of 3) than the value (6).

The prediction (15) [more generally, the exact proportionality (F1) between increments of elevation and chemical potential] depends crucially on the absence of thermal gradients. When thermal gradients are present, it is necessary to use (F5) in place of (F1). In CO_2, for which at the critical point[17,22] $(\partial P/\partial T)_\rho = 6.99 P_c T_c^{-1} = 1.7\times10^6$ erg/cm^3 deg, a gradient $T_z \simeq +0.6$ mdeg/cm (top of the cell warmer than the bottom) could account for the discrepancy between the observed density profile and that predicted by (15). A thermal gradient of this magnitude appears to have been within the limits of accuracy of the temperature measurements in the experiments.[21]

VII. SUSCEPTIBILITY AND SCATTERING PROFILES

Expressions (B1b), (B6), (15) can be solved to find the dependence of the susceptibility of the ideal critical fluid on height at constant temperature. For $\Delta T > 0$, the prediction to first approximation in $(\Delta z)^2$ is (ignoring the small dependence of χ on θ^2 at constant r)

$$\chi_a = \frac{g\rho_c^2}{aP_c}\left(\frac{\Delta T}{T_c}\right)^{-\gamma}\left[1 - \frac{\gamma b^2}{a^2}\left(\frac{\Delta T}{T_c}\right)^{-2(\gamma+\beta)}\left(\frac{\Delta z}{z_0}\right)^2\right]. \tag{18}$$

Since the intensity of light scattered from each element of a fluid is proportional to the susceptibility,[1-3] this leads to the prediction of scattered light profiles of approximately the form (18).

The prediction (18) for the choice of constants (4), (6) is compared with the authors' light-scattering measurements[23] in Fig. 6. The solid curves are experimental. Each dashed curve corresponds to Eq. (18) multiplied by a constant scale factor to bring the top of the curve into coincidence with the peak scattered intensity at the same temperature. A smaller scale factor is required for the upper curve (smaller ΔT) than for the lower curve.

The need for different scale factors and other discrepancies between the susceptibilities given by (18) and the measured scattered intensities are qualitatively those to be expected to result from the partial extinction of incident and scattered light which occurs in a finite thickness of fluid near the critical point. The extinction causes a reduction of observed scattered intensity. The fraction of the incident and scattered light re-

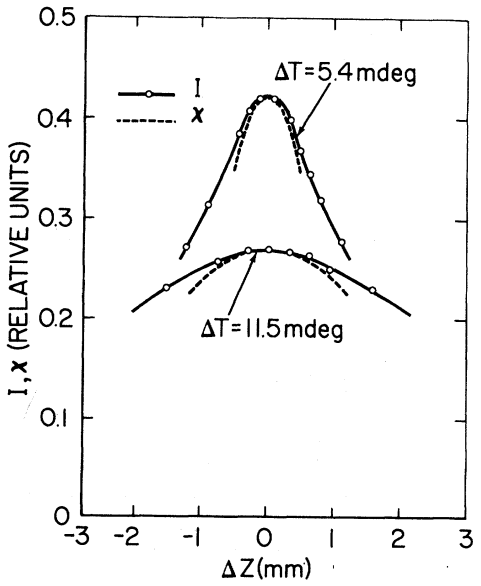

FIG. 6. Scattered intensity I and susceptibility χ as functions of height. The solid curves give intensities observed at 13.5° scattering angle; each dashed curve corresponds to Eq. (18), multiplied by an arbitrary constant. See text.

moved by extinction increases as the critical point is approached more closely. Consequently, within an isothermal sample the extinction increases to a maximum value that is characteristic of the particular temperature as the "critical height" ($z = z_c$, $\rho = \rho_c$) is approached either from above or below. The effect of the height-dependent extinction on the scattering profiles observed in a sample of fluid of finite thickness is therefore a decrease in the amplitude of the top of each profile relative to the amplitude of the wings, combined with an over-all reduction of height which is dependent on temperature. These features are apparent in Fig. 6 which, in effect, compares profiles measured for a sample of finite thickness (solid lines) to profiles that would be predicted for an ideally thin sample of the same fluid (dashed lines) if the amplitudes of the latter profiles are "corrected" by temperature-dependent factors to bring the peak intensities into coincidence with those of the observed profiles. The need for the temperature-dependent correction factors is also apparent in the figure, which shows that the ratio of observed peak intensities (solid curves) differs by a factor less than 2 [and considerably less than predicted by Eq. (18)] for a larger-than-2 ratio in the temperature distances from the critical point.

Quantitatively, the magnitude of the corrections for extinction, as also those for (a) angular anisotropy of the scattering and (b) multiple scattering, depends nonlinearly on the magnitude of the susceptibility and on the correlation range. A fuller discussion of these corrections may be found in Ref. 13, where an attempt was made to calculate them on the basis of estimates for the magnitude of the susceptibility and the correlation length close to the critical point.

VIII. CONTOURS OF CONSTANT WAVE SCATTERING

Equations (B1b) and (15) define temperature and height coordinates of contours of constant susceptibility (B6). Typical contours are shown in Figs. 1(d) and 7(a). These contours are approximated rather closely by contours of constant r [Fig. 7(b)]. They can be expected also to approximate contours of constant correlation length ξ. Wave scattering from each element of the fluid and corrections for finite sample thickness depend principally on the range of correlation and the susceptibility at each element. Therefore it can be expected that to a good approximation contours of constant scattering from elements of the fluid are simultaneously contours of constant corrections to scattering, and hence should coincide with contours of constant observed scattering, obtained from samples of finite thickness. Conversely, it can be predicted that contours of constant observed scattering should be contours of constant corrections to scattering, and hence contours of constant susceptibility and constant correlation range.

This prediction is compared with recent experimental results[23] in Figs. 8(a) and 8(b). The contours shown are the contours of constant r predicted by Eqs. (B1b) and (15) for the choice of constants (4), $\gamma = 1.20$, $a = 20$, and $T_c = 31.0027$°C. The data have been taken from individual isothermal profiles and refer [Fig. 8(a)] to the intensity[13] I of light scattered through an angle of 13.5°, and [Fig. 8(b)] to the inverse of the Rayleigh linewidth[26] (fluctuation decay rate) of this scattered light. It will be noticed[23] that to within the precision of these measurements, the intensity contours and contours of constant fluctuation decay times are of the same form. This confirms by light-scattering measurements a similarity of scaling-law behavior for equilibrium and nonequilibrium properties demonstrated by Sengers and Keyes in their analysis of thermal-conductivity data for CO_2.[27]

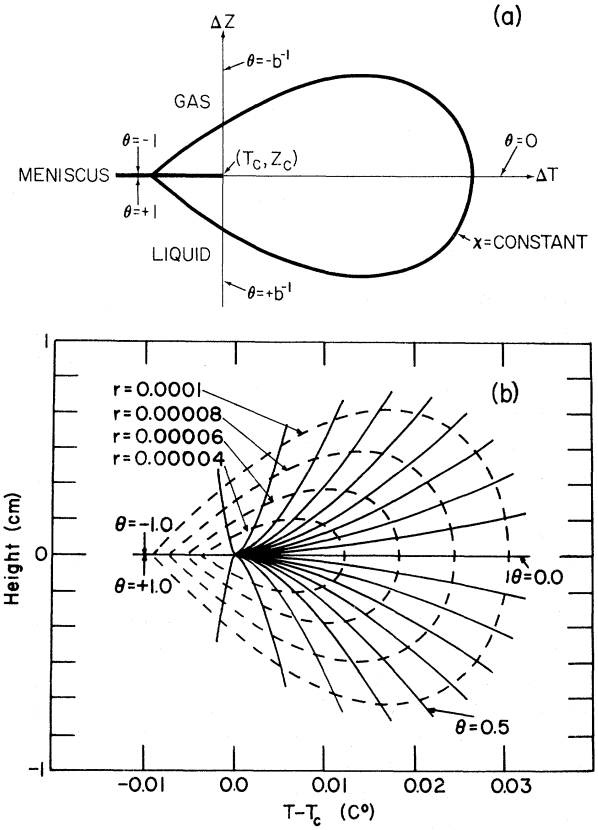

FIG. 7. (a) Contour of constant susceptibility ($r \simeq$ const) as a function of temperature ΔT and height Δz. (b) Contours of constant r (dashed lines) and constant θ (solid lines) for $T_c = 304$ °K, $b^2 = 1.3$, $a = 21$, $z_0 = 1.61 \times 10^5$ cm, and $\gamma + \beta = 1.55$ [Eqs. (B1b) and (15)].

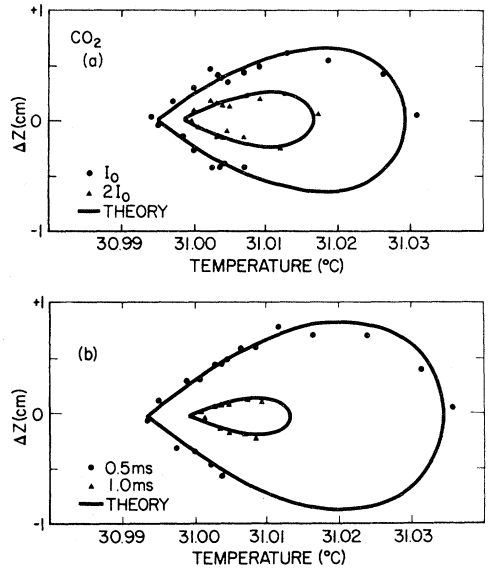

FIG. 8. Contours of constant wave scattering: (a) intensity; (b) inverse Rayleigh linewidth. Solid curves are contours of constant r, plotted for $T_c = 31.0027\,^{\circ}\mathrm{C}$. Values of r have been assigned arbitrarily in (a) and have been set equal to $(\tau/\tau_0)^{-1/\nu}$ in (b), with $\tau_0 = 1.55\ \mu\mathrm{sec}$, $\nu = 0.63$.

The contours of constant r shown in Figs. 7(b), 8(a), and 8(b) have an aspect ratio

$$\frac{\Delta z_{\max}}{\Delta T_{\max}} = a r^{\gamma+\beta-1} z_0 T_c^{-1} \frac{2}{3}\left(\frac{1}{3}\right)^{1/2}. \tag{19}$$

Here $\Delta z_{\max}$ is the maximum value of $z - z_c$ and $\Delta T_{\max}$ is the maximum value of $T - T_c$ for each contour. [Equation (19) follows immediately from Eqs. (B1b) and (15).] The choice of parameters (7) and (12) leads to slightly smaller aspect ratios than those shown in Figs. 8(a) and 8(b). Susceptibility contours, derived from Eq. (B6), have a slightly different shape (longer and narrower) and slightly smaller aspect ratio than contours of constant r. The combined effect of the two corrections [use of Eq. (B6) and parameters (7) and (12)] amounts to ~10% deviations from the contours exhibited in Figs. 8. Existing data, shown in Fig. 8, confirm the general correctness of the theory and of the estimates of parameters arrived at from a consideration of other data, mostly obtained farther from the critical point, but are insufficiently precise to lead to a definitive test or refinements of those results. An order-of-magnitude improvement of experiments of this type appears readily attainable, however, and could lead to significant new tests of the behavior of a fluid close to its critical point. Experiments directed to this end are currently in progress, and will be reported elsewhere.

IX. CONCLUSIONS

We have argued that in carbon dioxide an expression for the free energy of the form (E3), (B3) can be found which predicts correctly the magnitude of the critical components of all bulk thermodynamic properties (compressibility, specific heat, chemical potential) and which is compatible with existing light-scattering measurements. In particular, no evidence is found to within the precision of available experimental data and the accuracy of this analysis for any departure from the fundamentally nonanalytic behavior of the thermodynamic functions close to the critical point and the simplicities of their behavior that are expressed in the recently discussed general laws of scaling, homogeneity, and universality.[28-30]

Quantitative comparisons of the simple formulation (B1), (B3) that incorporates these laws with experimental data have shown that for the (first-approximation) choice of the five dimensionless constants that appear in the model expression (B3) for the free energy, namely, $b^2 = g = 1.3$, $a = 21$, $\beta = 0.35$, $\gamma = 1.20$, and for a constant background contribution to the specific heat, agreement with most of the measurements in the range $3\times10^{-5} < r < 3\times10^{-2}$ is within ~10%. Improved agreement (~5%) is obtained for the choice $\beta = 0.347$, $\gamma = 1.217$, $a = 22$, and a constant background for the specific heat. Agreement is to better than 5% with both branches of the specific-heat curve and with some of the most accurate PVT data close to the critical point. Disagreement tends to be greatest at the largest temperature and density distances from the critical point, where perfect scaling symmetries begin to break down. Further improvement can be obtained by employing background contributions that change gradually with temperature and density or by making small changes in the form of the model equations of state,[11,18,19,25] possibilities that have not been analyzed in detail here. For the model (B1), (B3) and either of the above choices of constants, the susceptibility and the correlation length vary by only a few percent over the full range of $-1 \leq \theta \leq +1$ for constant r; hence this r, the "distance" from the critical point, is in the model used here a measure to a first approximation of the mean range of local correlations and, via the equivalence of contours shown in Figs. 8(a) and 8(b), also a measure to a first approximation of the mean time for growth and decay of fluctuations of localized ordering.

The numerical values of the exponents considered here differ significantly from the values $\beta = 0.3125$, $\gamma = 1.25$ predicted by the Ising model of the critical region. It may be noted that a value of $\gamma < 1.20$ is found when experimental data obtained close to

the critical point are ignored or assigned a reduced weight. A possible increase of γ to $\gamma > 1.22$ and simultaneous decrease of β to appreciably less than 0.35 very close to the critical point may have been missed in the experimental investigations analyzed in this paper; questions of this kind may be resolved through refinements of the technique and analysis of measurements of the type described by Eqs. (18) and (19) of this paper.

ACKNOWLEDGMENTS

The authors wish to thank Professor Michael Fisher for suggesting the use of a Josephson-Schofield representation for the analysis of the data, J. V. Sengers for providing them with a preliminary analysis (unpublished) of PVT data, and both J. V. Sengers and J. M. H. Levelt Sengers for helpful discussions. One of the authors (J.W.) is indebted to Professor George Benedek and his colleagues in the Department of Physics of the Massachusetts Institute of Technology for their hospitality and helpful discussions during an extended visit, and wishes, in particular, to acknowledge valuable discussions on the subject of this paper with Professor J. D. Litster. Finally, the authors thank Robert Freeman for his assistance with the experiments and Richard Marth for computational assistance.

APPENDIX A: GENERAL THERMODYNAMIC RELATIONS AND DEFINITIONS

For convenience of reference we summarize here the definitions and derivations of the thermodynamic quantities required for the present investigation.

At thermodynamic equilibrium, the energy E of a fixed quantity of fluid at temperature T, entropy S, pressure P, volume V, obeys the second law of thermodynamics in the form

$$dE = T\,dS - P\,dV. \tag{A1}$$

As a consequence, its Gibbs free energy,

$$G = E - TS + PV = \mu N \tag{A2}$$

(N is the number of particles, μ the chemical potential per particle), is a function of the intensive variables T and P,

$$dG = N\,d\mu = -S\,dT + V\,dP, \tag{A3}$$

and its Helmholtz free energy per unit volume,

$$f = F/V = e - Ts = \mu\rho - P. \tag{A4}$$

($e = E/V$, $s = S/V$, $\rho = N/V$), is a function of density and temperature,

$$df = \mu\,d\rho - s\,dT. \tag{A5}$$

Expression (A5) for the Helmholtz energy follows from the Gibbs-Duhem relation (A3), which requires

$$dP = \rho\,d\mu + s\,dT. \tag{A6}$$

The Helmholtz energy can be used to generate all thermodynamic functions of interest.

First derivatives of the Helmholtz free energy yield expressions for the chemical potential,

$$\mu = \left(\frac{\partial f}{\partial \rho}\right)_T, \tag{A7a}$$

and entropy,

$$s = -\left(\frac{\partial f}{\partial T}\right)_\rho, \tag{A7b}$$

as functions of temperature and density. Higher derivatives give the isothermal compressibility,

$$K_T = -\frac{1}{V}\left(\frac{\partial V}{\partial P}\right)_T = \frac{1}{\rho}\left(\frac{\partial \rho}{\partial P}\right)_T = \frac{1}{\rho^2}\left(\frac{\partial \rho}{\partial \mu}\right)_T, \tag{A7c}$$

or susceptibility,

$$\chi = \rho^2 K_T = \left(\frac{\partial \rho}{\partial \mu}\right)_T, \tag{A7d}$$

and the specific heat at constant density,

$$c_\rho = \frac{C_V}{V} = T\left(\frac{\partial s}{\partial T}\right)_\rho. \tag{A7e}$$

The latter two quantities are of particular interest because they both diverge at the critical point ($\rho = \rho_c$, $T = T_c$)—the specific heat weakly, the susceptibility (compressibility) strongly.

APPENDIX B: THERMODYNAMICS OF LINEAR MODEL

The general parametric equations of state of the linear model of Schofield[6] written in a form applicable to fluids are

$$\Delta\rho = g\rho_c r^\beta \theta, \tag{B1a}$$

$$\Delta T = T_c r(1 - b^2\theta^2), \tag{B1b}$$

$$\Delta\mu = aP_c\rho_c^{-1} r^{\beta+\gamma}(\theta - \theta^3), \tag{B1c}$$

where ρ_c, T_c, P_c are, respectively, the density, temperature, and pressure at the critical point. Here $\Delta\rho = \rho - \rho_c$, $\Delta T = T - T_c$; and $\Delta\mu = \mu(\rho, T) - \mu(\rho_c, T)$ is the anomalous part of the chemical potential. The quantities g, β, b^2, a, and γ are dimensionless constants, with $b^2 > 1$.

In the restricted linear model,[7] b^2 is related to the exponents β and γ (Appendix B C). In the unrestricted linear model, b^2 is an adjustable constant. The exponents β, γ, and $\delta = (\gamma/\beta) + 1$ are particularly significant in that they characterize the shape of the coexistence curve (β), the degree of the critical isotherm (δ), and the divergence of the isothermal compressibility, K_T, along the

critical isochore (γ). Certain characteristics of the linear model are illustrated pictorially in Figs. 1 and 3. Of particular interest are contours of constant inverse susceptibility, χ^{-1} [Eq. (A7d)], which, for special choices of b^2, are approximately coincident with contours of constant r in the immediate vicinity of the critical point [see Sec. II and Eq. (B6)]. A typical constant χ^{-1} contour as seen when viewed along the three axes in μ-ρ-T space is illustrated in Fig. 1. Figure 3 illustrates contours of constant r and constant θ projected onto the T-ρ plane for a particular choice of g and b^2 as well as the particular values of θ that yield the critical isochore ($\theta=0$), the critical isotherm ($\theta=1/b$), and the coexistence curve ($\theta=1$). In particular, the coexistence curve ($\theta=\pm1$) is of the form [from (B1a), (B1b)]

$$\text{coexistence boundary: } \Delta\rho=\pm g\rho_c[(1-b^2)^{-1}\Delta T/T_c]^{\beta}. \tag{B2}$$

Equations (B1a), (B1b), and (B2) are identical to Eqs. (1a), (1b), and (2) of the text.

A. Single-phase region

It is readily verified from Eq. (A7a) (Appendix A) that Eq. (B1c) corresponds to a contribution to the free energy of the form[15]

$$f_a=agP_c r^{\gamma+2\beta}f(\theta), \tag{B3a}$$

where

$$f(\theta)=\sum f_n\theta^n=f_0+f_2\theta^2+f_4\theta^4. \tag{B3b}$$

(A complete expression for the free energy contains in addition background terms, discussed in Appendix E). The dimensionless constants f_n in (B3b) are functions of b^2, β, γ (Table IV).[31] It is to be noted that the free energy (B3) is analytic everywhere in the single-phase region except at the critical point ($r=0$), where there is an essential singularity.

Other thermodynamic quantities of interest can be derived from (B3) using Eqs. (A7) (Appendix A). The results are as follows:

$$s_a=-agP_cT_c^{-1}r^{\gamma+2\beta-1}s(\theta), \tag{B4a}$$

$$T^{-1}(c_\rho)_a=-agP_cT_c^{-2}r^{\gamma+2\beta-2}c(\theta), \tag{B5a}$$

$$(\chi^{-1})_a=aP_cg^{-1}\rho_c^{-2}r^{\gamma}\chi^{-1}(\theta), \tag{B6a}$$

where

$$s(\theta)=s_0+s_2\theta^2, \tag{B4b}$$

$$c(\theta)=(1-d^2\theta^2)^{-1}(c_0+c_2\theta^2), \tag{B5b}$$

$$\chi^{-1}(\theta)=(1-d^2\theta^2)^{-1}(1+\chi_2^{-1}\theta^2+\chi_4^{-1}\theta^4). \tag{B6b}$$

Here $d^2=b^2(1-2\beta)$ and the coefficients s_n, c_n, χ_n^{-1} depend on b^2, β, γ (Table IV).

From (E5) (Appendix E), (B1c), and (B3) it follows that the pressure contains a nonanalytic part of the form

$$P_a=(\rho_c+\Delta\rho)\mu_a-f_a$$
$$=aP_cr^{\gamma+\beta}(\theta-\theta^3)-agP_cr^{\gamma+2\beta}[f_0+(f_2-1)\theta^2+(f_4+1)\theta^4]. \tag{B7}$$

The single-phase region is bounded by a two-branched contour $\theta=-1$ (gas) and $\theta=+1$ (liquid). On this contour, at constant temperature, it is evident that $(\mu_a)_{\text{gas}}=(\mu_a)_{\text{liquid}}$ and $(P_a)_{\text{gas}}=(P_a)_{\text{liquid}}$. Hence this contour is the boundary of coexisting gas and liquid phases.

TABLE IV. Coefficients for use in Eqs. (B3)–(B6). Here $\alpha=2-\gamma-2\beta$ and $d^2=b^2(1-2\beta)$.

$f_0=\dfrac{b^2\gamma\alpha-\gamma+2\beta}{2b^4\alpha(1-\alpha)(2-\alpha)}$	$s_0=(2-\alpha)f_0$
$f_2=\dfrac{\gamma-2\beta-d^2\alpha}{2b^2\alpha(1-\alpha)}$	$s_2=\dfrac{\gamma-2\beta}{2\alpha b^2}$
$f_4=\dfrac{-d^2}{2\alpha b^2}$	$c_0=(1-\alpha)s_0$
	$c_2=(\gamma-1)s_2$
$\chi_2^{-1}=-3+b^2(-1+2\gamma+2\beta)$	$\chi_4^{-1}=b^2(3-2\gamma-2\beta)$

B. Two-phase region

Inside this boundary, in the region of coexisting liquid and gas phases, expressions (B1) apply to each phase separately, with $\theta=+1$ for the liquid and $\theta=-1$ for the gas. In this region the chemical potential (A2) is a function only of temperature and is equal to its value at the coexistence curve. In the linear model, $\Delta\mu=0$ at $\theta=\pm1$. Hence $\Delta\mu=0$ everywhere in the two-phase region [in agreement with Eq. (E2) of Appendix E if $\chi_b^{-1}=0$ for this region], and f_a in this region is, from (B3) and (B1b),

$$(f_a)_{\text{two phase}}=agP_c\left(\frac{\Delta T}{(1-b^2)T_c}\right)^{\gamma+2\beta}(f_0+f_2+f_4). \tag{B8}$$

Successive differentiations of (B8) lead to expressions for the entropy and specific heat in the two-phase region. Of particular interest is the specific heat,

$$\left(\frac{(c_\rho)_a}{T}\right)_{\text{two phase}}=-\frac{(\gamma+2\beta)(\gamma+2\beta-1)}{\Delta T^2}(f_a)_{\text{two phase}}. \tag{B9}$$

The specific heat is greater in the two-phase region than in the single-phase region at the same temperature close to the phase boundary. (By contrast, the entropy does not change discontinuously at the boundary of the region of coexisting phases; it has the same value in the two-phase region as in a single phase at the same temperature at $\theta = \pm 1$.)

C. Restricted linear model

Some special choices of the constants b^2, β, γ merit comment. For $\beta+\gamma=\frac{3}{2}$ and $\gamma b^2=\frac{3}{2}$, the dependence on θ of the susceptibility (B6b) disappears, as does that of the specific heat (B5). [For $\beta+\gamma=\frac{3}{2}$, the isothermal integration of Eq. (C2), Appendix C, yields Eq. (C4) exactly, with $\gamma b^2=\frac{3}{2}$.[8,11]] The specific heat continues to be independent of θ for $\beta+\gamma\neq\frac{3}{2}$ for the "restricted" linear model, in which $b=b^*$, where[7]

$$(b^*)^2=\frac{\gamma-2\beta}{\gamma(1-2\beta)}=\frac{\delta-3}{(\delta-1)(1-2\beta)}, \tag{B10}$$

with $\delta=(\gamma/\beta)+1$.

The discussion elsewhere in this paper does not assume either $\beta+\gamma=\frac{3}{2}$ or $b=b^*$; these relationships are satisfied approximately but not exactly.

D. Topography of parametric models; metastable states and spinodal

For $T<T_c$, Eqs. (1) lead to values of $|\Delta\rho|$ that are never smaller than those which correspond to $|\theta|=|\theta_m|=d^{-1}=[b^2(1-2\beta)]^{-1/2}$. It is seen from Eqs. (B5) and (B6) that on the boundary $\theta=\theta_m$, for particular choices of b^2, β, and γ, both the inverse susceptibility and the specific heat diverge and change sign. Divergence of the inverse of the susceptibility (infinite rigidity) is not an observed behavior of accessible states of real fluids. For other choices of b^2, β, and γ compatible with experiment, the susceptibility diverges before $|\theta|$ reaches $|\theta_m|$, at a boundary $|\theta|=|\theta_n|$, with $|\theta_n|<|\theta_m|$. The boundary at $|\theta|=|\theta_n|$ resembles a classical spinodal line. This leaves open the possibility of a region $1<\theta^2<\theta_n^2$ of *metastable* gas or liquid which behaves as an ideal single-phase fluid, and whose thermodynamic properties in this region continue to obey Eqs. (B3)–(B6) rather than Eqs. (B8), (B9), etc.

In the limit $b\to b^*$ (Appendix B C), the boundaries θ_m and θ_n merge into a single boundary of metastable behavior along which both the specific heat and the susceptibility remain finite, with an infinite derivative in the susceptibility[7] and a cusp in the chemical potential at this boundary. For $b<b^*$ (as is the case for the values of b, β, and γ found in this investigation) the boundary $|\theta_n|$ is reached before $|\theta_m|$. For $b>b^*$, as suggested in some previous investigations,[16] the boundary $|\theta|=|\theta_n|$ is not reached before $|\theta_m|$, and there is no accessible spinodal line or boundary of metastable behavior in the above sense; rather, the susceptibility then remains finite for all $|\theta|<|\theta_m|$, and decreases to zero at $|\theta|=|\theta_m|$, a situation that seems unphysical. It is to be noted, finally, that for the Ho-Litster[9] "cubic-model" modification (end of Appendix C) that leads to $\chi\propto r^{-\gamma}$ as an exact result,[32] the susceptibility has an infinite derivative and the chemical potential has a cusp just as in the restricted linear model in the limit $b\to b^*$.[25]

APPENDIX C: DERIVATION OF PARAMETRIC REPRESENTATION FROM SUSCEPTIBILITY DATA

A. Natural variables for use close to critical point

The particular parametric representation postulated for use in the analysis presented in this paper can also be derived from experiment. Key features of the experimental data are shown in Fig. 2. The coexistence curve and contours of constant susceptibility shown in Fig. 2 are not perfectly symmetric about the critical density. However, to the extent that the contours are symmetric (the smaller susceptibility contours in particular are quite symmetric) they can be characterized approximately by the following empirical relationships[11]:

$$\chi\propto(T_p-T_c)^{-\gamma}, \tag{C1a}$$

$$|\Delta\rho|\propto(-\Delta T)^{\beta}\quad\text{coexistence boundary,} \tag{C1b}$$

$$|\Delta\rho|\propto(T_p-T)^{q}(T_p-T_c)^{\beta-q}\quad\text{susceptibility contour.} \tag{C1c}$$

Here $\Delta\rho=\rho-\rho_c$, $\Delta T=T-T_c$; T_p is the maximum temperature on a susceptibility contour; and[11] $\gamma\approx1.2$, $q\approx0.5$, $\beta\approx0.35$.

For $q=\frac{1}{2}$, and with the substitution of parametric variables r and θ defined through the relations $(T_p-T)(T_p-T_c)^{-1}=b^2\theta^2$ and $T_p-T_c=T_1 r$, expressions (C1a) and (C1c) become

$$\chi=\chi(r)=\chi_1 r^{-\gamma} \tag{C2a}$$

and

$$\Delta\rho(r,\theta)=\rho_1 r^{\beta}\theta, \tag{C2b}$$

with

$$\Delta T(r,\theta)=T_1 r(1-b^2\theta^2). \tag{C2c}$$

Here b^2 is a dimensionless constant and χ_1, ρ_1, and T_1 are constants with dimensions of susceptibility, density, and temperature, respectively. The latter two equations [(C2b) and (C2c)] are equivalent to Eqs. (1) of the text.

It is evident that in this representation, illustrated in Fig. 3, the parameter r is constant on each contour of the type (C1c). The magnitude of r grows in proportion to $T_p - T_c$; that is, r grows in proportion to the "remoteness" of the contour from the critical point. The parameter θ is proportional to the macroscopic order parameter $\Delta\rho$ at constant r; the average "order," θ, increases from left to right along each contour of given r. A constant value of $|\theta|$ with $b^2\theta^2 > 1$ corresponds to the boundary, (C1b), of the region of coexisting phases.

The parameter r as specifically defined above is closely related to both the susceptibility at equilibrium of the macroscopic thermodynamic state and the microscopic range ξ of transient spontaneous ordering. According to the approximate representations (C1c) and (C2) of the experimental data for CO_2, contours of constant r as defined above are contours of almost constant susceptibility. In accordance with the expected dependence of the susceptibility on ξ,[2,3] it may be conjectured that these contours are also contours of nearly constant ξ.

It is known that along the critical isochore ($\Delta\rho = 0$) the dependence of ξ on temperature is of the form[3,14,26] $\xi \propto (T - T_c)^{-\nu}$. [The exponent ν is found both theoretically and experimentally to satisfy the relation $\gamma \approx 2\nu$ or, more exactly,[3] $\gamma = (2 - \eta)\nu$, with $\eta \sim 0.1$[3,14,26,33]]. Consequently, the parameter r as defined above can be given the following alternative interpretations:

$$\text{Macroscopic:}\quad r \simeq (\chi/\chi_1)^{-1/\gamma}, \tag{C3a}$$

$$\text{Microscopic:}\quad r \simeq (\xi/\xi_1)^{-1/\nu}. \tag{C3b}$$

The empirical statements (C1) and the assignment $q = \frac{1}{2}$ are approximations. Consequently, not all of Eqs. (C2) and the deductions based on them should be expected to exactly characterize a real fluid, such as carbon dioxide. Equations (C1) and their consequences, (C2) *et seq.*, serve, rather, as simple approximately correct characterizations of the critical region that can be perfected through comparisons with more exact experimental data and refinements of theory.

By using the linear model to fit the data we have effectively retained equations (C2b) and (C2c) as exactly correct equations of transformation from conventional ρ, T to parametric r, θ variables. However, we have chosen the constants in those transformation equations to meet our requirement that the susceptibility be mainly a function of r and thus maintain the approximate validity of (C2a) and of the interpretations based on Eq. (C2a) that have been discussed above.

B. Equation of state close to critical point

Isothermal integration of (C2a), using (C2b) and (C2c), leads to a nonanalytic component of the chemical potential (E2) (Appendix E) which includes as a factor an infinite series in θ.[34] A good approximate representation of the result of this integration, for a choice of constants that leads to $\theta_{\text{gas}} \approx -1$, $\theta_{\text{liquid}} \approx +1$, is

$$\Delta\mu(\rho, T) = \mu(\rho, T) - \mu(\rho_c, T) = \mu_1 r^{\gamma+\beta}(\theta - \theta^3), \tag{C4}$$

with $\mu_1 = \text{const}$. (Higher-order terms in the infinite series in θ vanish identically for $\gamma + \beta = 1.5$, and they are still quite small for $1.5 < \gamma + \beta < 1.6$, an inequality that is almost certainly satisfied for CO_2.)

The simple expression (C4) is equivalent to the "linear-model" expression (B1c). A second integration of (C2a) will be found to give an expression for the free energy (E3) that, with an appropriate choice for $f(\rho_c, T)$, reduces to a sum of just three terms equivalent to Eq. (B3) in the approximation (C4).

The simplified expression on the right-hand side in (C4) is of the form introduced *a priori* by Schofield in his theory of the critical region of magnets and fluids[6] (Appendix B). Equation (C2c) with a general choice of b^2 was also postulated by Schofield, and Eq. (C2b) is equivalent to the "linear-model" specialization of his general parametric expression for the density of a fluid. The above discussion shows that for a special choice of b^2, (C4) [or equivalently (B1c)] can be derived for fluids from empirical data, summarized by the approximate expressions (C1), in a manner compatible with retention of all of expressions (C2) and (C3) as *approximately* correct statements.

The use of (C4) as an *exact* model equation requires a modification of at least one of the three expressions (C2). However, since the required modification is small for appropriate choices of the constants of the transformation, we have used the simple "linear model" of Schofield with constants chosen to preserve (C2a) as an approximate, but not exact, equality, in the expectation that any further modification of Eqs. (C2)–(C4) for use close to the critical point of CO_2 will be small.

An example of a small modification to the parametric equations we have presented is the "cubic-model" parametrization of Ho and Litster[9] in which a factor $(1 + c\theta^2)$ is included on the right-hand side of (C2b) [or equivalently (1a)]. With this inclusion, and with the temperature and chemical potential given by (C2c) and (C4), respectively, Eq. (C2a) can be retained as an exact result compati-

ble with the parametrization of $\Delta\mu$, ΔT, and $\Delta\rho$, provided that[32] $b^2 = b^2_{\rm HL} = 3/(3-2\beta)$ and $c = [2(\gamma+\beta)-3]/(3-2\beta)$. For the values of γ and β used in this paper, $b^2_{\rm HL} = 1.30$, which is also the value of b^2 that has been used in this paper because it provides the best over-all fit to the coexistence curve and to the susceptibility contours (see Sec. II), and $c \simeq 0.05$.

APPENDIX D: ALTERNATIVE REPRESENTATIONS OF MEASURED SPECIFIC HEAT

The result of measurements[20] of the specific heat of CO_2 over the range of temperatures $4\times10^{-5} < |\Delta T/T_c| < 10^{-2}$ is summarized in Eq. (8) in the text. Apart from a factor $T/T_c \simeq 1$, that expression is of the form

$$\frac{C_V}{V} = (A_0 t^{-\alpha_0} + B_0)\frac{P_c}{T_c}\frac{T}{T_c}, \tag{D1}$$

where $t = |\Delta T/T_c|$. Equation (D1) closely resembles the theoretical expressions Eqs. (13) and (B9) of the text, with the addition of background contributions. A comparison with the experimental results (8) (using $R = 8.314$ JK^{-1} mol^{-1}, $T_c = 304$ K, $P_c = 72.9$ atm $= 7.38$ J/cm^3, $m\rho_c = 0.468$ g/cm^3, and a molar mass equal to 44 g) leads to the following values for the constants A_0, B_0, and α_0:

$$\begin{aligned} &A_{0+} = 20.3, \quad A_{0-} = 38.1, \\ &B_{0+} = -12.6, \quad B_{0-} = -0.087, \\ &\alpha_0 = 0.125. \end{aligned} \tag{D2}$$

The following modified form of Eq. (D1) has been used to represent the experimental data approximately, in a form more readily compared with theory when $\alpha = \alpha' \neq \alpha_0$:

$$\frac{C_V}{V} = (A' t^{-\alpha'} + B')\frac{P_c}{T_c}\frac{T}{T_c}, \tag{D3}$$

where

$$A' = A_0 \frac{t_1^{-\alpha_0} - t_2^{-\alpha_0}}{t_1^{-\alpha'} - t_2^{-\alpha'}}, \tag{D4a}$$

$$B' = A_0 t_2^{-\alpha_0} - A' t_2^{-\alpha'} + B_0. \tag{D4b}$$

It is to be noted that expression (D3) is equivalent to (D1) at all temperatures for $\alpha' = \alpha_0$ and that it is also equal numerically to (D1) for any $\alpha' \neq \alpha_0$ at the two temperatures $t = t_1$ and $t = t_2$. Because of these features, (D3) can provide nearly as good a representation of the data as expressions (D1) or (8) for appreciable ranges of α' and t. In particular, for the choices $t_1 = 7\times10^{-5}$ and $t_2 = 2.5\times10^{-3}$, the agreement between (D1) and (D3) is ~1% for values of α' as small as 0.08 and for temperatures in the range $4\times10^{-5} < t < 5\times10^{-3}$. This range of temperatures includes most of the specific-heat data reliable to ~1%.[20] Values of A' and B' calculated from experiment for this choice of values for t_1 and t_2 and representative choices of α' are tabulated in Table V.

The corresponding values of $A_\pm$ and $B_\pm$ for use in Eq. (8) are smaller than the A' and B' values listed in the table by a factor $VP_c/RT_c = 0.275$.

APPENDIX E: SEPARATION OF ANOMALIES FROM BACKGROUND

A rigorous discussion of critical-point anomalies requires consideration of nondivergent and analytic contributions to thermodynamic properties, in addition to the divergent and nonanalytic ones represented by the equations of the parametric models. Detailed discussions of extensions of the model equations have been presented elsewhere.[18,19,25] For present purposes, it is sufficient to imagine each thermodynamic function divided into two parts: (a) a portion that contains the anomalous rapidly varying behavior typical of the critical point; and (b) background terms that are small and/or slowly varying near the critical point.

It is convenient to begin this discussion by expressing the inverse of the susceptibility (A7d) as

$$\chi^{-1} = \left(\frac{\partial\mu}{\partial\rho}\right)_T = (\chi^{-1})_a + (\chi^{-1})_b. \tag{E1}$$

Here $(\chi^{-1})_a$ contains the essential singularity characteristic of the anomalous behavior of the compressibility in the vicinity of the critical point, and $(\chi^{-1})_b$ is a background term that is negligibly small at the critical point and expresses all departures from ideal critical behavior that appear at appreciable distances from the critical point. Using this decomposition, it is possible to discuss anomalies that occur close to the critical point without reference to thermodynamic behavior farther from the critical point. In this representation the latter behavior appears explicitly as a small perturbation to be added to "ideal" critical-point anomalies; the "background" terms contribute only secondarily to the critical-point phenomena treated in the present investigation, but are required to assure a smooth and orderly transition from the universal laws of behavior charac-

TABLE V. Values of A' and B' calculated from experiment for $t_1 = 7\times10^{-5}$ and $t_2 = 2.5\times10^{-3}$, and for representative choices of α'.

α'	A'_+	A'_-	B'_+	B'_-
0.08	45.3	84.9	−42.8	−56.6
0.10	31.0	58.1	−26.0	−25.3
0.125	20.3	38.1	−12.6	−0.087

teristic of all substances close to their critical points to the less easily characterized and substance-specific laws of behavior that apply to liquids and gases far from their critical points.

Successive integrations of χ^{-1} at constant temperature lead to expressions for the critical and background components of the chemical potential and free energy:

$$\mu = \int \chi^{-1}\, d\rho$$

$$= \int_{\rho_c}^{\rho} (\chi^{-1})_a\, d\rho + \int_{\rho_c}^{\rho} (\chi^{-1})_b\, d\rho + \mu(\rho_c, T)$$

$$= \mu_a + \mu_b, \tag{E2}$$

$$f = \int \mu\, d\rho = \int_{\rho_c}^{\rho} \mu_a\, d\rho + \int_{\rho_c}^{\rho} \mu_b\, d\rho + f(\rho_c, T)$$

$$= f_a + f_b. \tag{E3}$$

The decomposition into f_a, f_b, and μ_a, μ_b is made in accordance with the requirements that f, f_a, and μ_a be analytic except at the critical point and μ_a and f_a correspond to $(\chi^{-1})_a$.

Since $\mu(\rho, T)$ must be analytic for all $\rho \neq \rho_c$ (except along the boundary of the region of coexisting phases) it follows that $\mu(\rho_c, T)$ is analytic for the choice $\Delta\mu(\rho, T)$ given in (C4). Consequently, the model expression for $\Delta\mu$ given in (C4) can be equated to μ_a in (E2). The term μ_b in (E2) then includes the (analytic) portion of $\mu(\rho, T)$ close to the critical point that is not dependent on density, namely, $\mu(\rho_c, T)$, in addition to all corrections to expression (C4) that are required at temperature and density distances remote from the critical point.

Successive differentiations of (E3) with respect to temperature give expressions for the entropy (A7b) and specific heat (A7a). It is to be noticed that the nonanalyticity in χ^{-1} leads, via (E2) and (E3), to the appearance of a nonanalytic component of the specific heat; the specific heat has an anomaly as a consequence of (and calculable from) the anomaly in the equation of state.

Other thermodynamic quantities can be divided similarly into singular and background components. As an example, we cite the pressure, given by

$$P = \mu\rho - f = P_a + P_b, \tag{E4}$$

where

$$P_a = \rho\mu_a - f_a \tag{E5a}$$

and

$$P_b = \rho\mu_b - f_b. \tag{E5b}$$

APPENDIX F: HEIGHT PROFILES

In a fluid at thermodynamic equilibrium in the presence of an external field of force (e.g., gravity) many of the thermodynamic properties vary with location in the fluid. For example, in the absence of forces other than gravity the pressure varies with height z in accordance with the relation $dP = -m\rho g_0\, dz$. Here g_0 is the acceleration of gravity and $m\rho$ the mass density of the fluid. As a consequence, the density, free energy, chemical potential, compressibilities, etc., are also functions of elevation within the fluid. From the Gibbs-Duhem relation, (A6), and the definition (E1) it follows that (a), for *constant temperature*,[35]

$$\frac{dP}{\rho} = d\mu = -mg_0\, dz = \chi^{-1}\, d\rho, \tag{F1}$$

whence

$$\Delta z = z - z_c = -\frac{1}{mg_0} \int_{\rho_c}^{\rho(z)} \chi^{-1}\, d\rho = \frac{\mu(\rho_c, T) - \mu(\rho, T)}{mg_0}, \tag{F2a}$$

where z_c is the "critical height" in the fluid, i.e., the height at which $\rho = \rho_c$. If $\mu(\rho_c, T)$ does not contribute to μ_a, then, from (E2), the integral on the right-hand side of (F2a) is equal to

$$\int_{\rho_c}^{\rho(z)} \chi^{-1}\, d\rho = \mu_a + \int_{\rho_c}^{\rho(z)} (\chi^{-1})_b\, d\rho. \tag{F2b}$$

If (b) the temperature is *not* constant, it follows from the Gibbs-Duhem relation (A6) and the identity

$$dP = \left(\frac{\partial P}{\partial \rho}\right)_T d\rho + \left(\frac{\partial P}{\partial T}\right)_\rho dT \tag{F3}$$

that

$$dP = -m\rho g_0\, dz = \rho \left(\frac{\partial \mu}{\partial \rho}\right)_T d\rho + \left(\frac{\partial P}{\partial T}\right)_\rho dT \tag{F4}$$

and hence

$$dz = -\frac{1}{mg_0} \left(\frac{\chi^{-1}\, d\rho}{1 + (m\rho g_0)^{-1} (\partial P/\partial T)_\rho\, T_z} \right), \tag{F5}$$

where $T_z = dT/dz$.

†Research supported by the National Science Foundation and the Office of Naval Research.

*Present address: Naval Ordnance Laboratory, Silver Spring, Md. 20910.

[1]A. Einstein, Ann. Phys. (Leipz.) 33, 1276 (1910).

[2]L. S. Ornstein and F. Zernike, Proc. Acad. Sci. Amsterdam 17, 793 (1914).

[3]M. E. Fisher, J. Math. Phys. 5, 944 (1964).

[4]K. Kawasaki, Ann. Phys. (N.Y.) 61, 1 (1970).

[5]B. D. Josephson, J. Phys. C 2, 1113 (1969).

[6]P. Schofield, Phys. Rev. Lett. 22, 606 (1969).

[7]P. Schofield, J. D. Litster, and J. T. Ho, Phys. Rev. Lett. 23, 1098 (1969).

[8]A. A. Migdal, Zh. Eksp. Teor. Fiz. 62, 1559 (1972) [Sov. Phys.—JETP 35, 816 (1972)].

[9]J. T. Ho and J. D. Litster, Phys. Rev. B 2, 4523 (1970).

[10]A. Michels, B. Blaisse, and C. Michels, Proc. R. Soc. Lond., Ser. A 160, 358 (1937); A. Michels, C. Michels, and H. Wouters, *ibid.* 153, 214 (1935).

[11]B. S. Maccabee and J. A. White, Bull. Am. Phys. Soc. 18, 725 (1973).

[12]J. M. H. Levelt Sengers, J. Straub, and M. Vicentini-Missoni, J. Chem. Phys. 54, 5034 (1971).

[13]J. A. White and B. S. Maccabee, Phys. Rev. Lett. 26, 1468 (1971).

[14]J. M. Lunacek and D. S. Cannell, Phys. Rev. Lett. 27, 841 (1971).

[15]P. C. Hohenberg and M. Barmatz, Phys. Rev. A 6, 289 (1972).

[16]T. A. Murphy, J. V. Sengers, and J. M. H. Levelt Sengers, in *Proceedings of the Sixth Symposium on Thermophysical Properties,* edited by P. E. Liley (American Society of Mechanical Engineers, New York, 1973).

[17]M. Vicentini-Missoni, J. M. H. Levelt Sengers, and M. S. Green, J. Res. Natl. Bur. Std. A 73, 563 (1969).

[18]M. S. Green, M. J. Cooper, and J. M. H. Levelt Sengers, Phys. Rev. Lett. 26, 492 (1971).

[19]B. S. Maccabee and J. A. White, Phys. Lett. 49A, 69 (1974).

[20]J. A. Lipa, C. Edwards, and M. J. Buckingham, Phys. Rev. Lett. 25, 1086 (1970).

[21]E. H. W. Schmidt, in *Critical Phenomena,* Natl. Bur. Std. Misc. Publ. 273, edited by M. S. Green and J. V. Sengers (U.S. GPO, Washington, D.C., 1966), p. 13.

[22]J. Straub, Chemie-Ing.-Techn. 39, 291 (1967).

[23]J. A. White, R. M. Freeman, and B. S. Maccabee, Bull. Am. Phys. Soc. 18, 725 (1973).

[24]We have profited from the use of a table of compressibility values derived from PVT data by J. V. Sengers (private communication).

[25]B. S. Maccabee and J. A. White (unpublished).

[26]B. S. Maccabee and J. A. White, Phys. Rev. Lett. 27, 495 (1971).

[27]J. V. Sengers and P. H. Keyes, Phys. Rev. Lett. 26, 70 (1971).

[28]L. P. Kadanoff, W. Gotze, D. Hamblen, R. Hecht, E. A. S. Lewis, V. V. Palciauskas, M. Rayl, J. Swift, D. Aspnes, and J. Kane, Rev. Mod. Phys. 39, 395 (1967).

[29]K. G. Wilson, Phys. Rev. B 4, 3174 (1971); 4, 3184 (1971).

[30]J. Hubbard, Phys. Lett. 40A, 111 (1972).

[31]Expressions in Table IV follow from the definitions (1), (A7), (E1)–(E3), and the chain rule for partial differentiation, e.g.,

$$\frac{\partial f}{\partial(\rho,T)}=\frac{\partial f}{\partial(r,\theta)}\frac{\partial(r,\theta)}{\partial(\rho,T)}.$$

The Jacobian corresponding to (1) is

$$\frac{\partial(\rho,T)}{\partial(r,\theta)}=\begin{pmatrix} g\beta r^{\beta-1}\theta\rho_c & g r^{\beta}\rho_c \\ (1-b^2\theta^2)T_c & -2b^2 r\theta T_c \end{pmatrix}$$

whence, by matrix inversion,

$$\frac{\partial(r,\theta)}{\partial(\rho,T)}=[1-b^2(1-2\beta)\theta^2]^{-1} \times\begin{pmatrix} 2b^2\theta r^{1-\beta}(g\rho_c)^{-1} & T_c^{-1} \\ (1-b^2\theta^2)r^{-\beta}(g\rho_c)^{-1} & -\beta\theta(rT_c)^{-1} \end{pmatrix}.$$

[32]The general cubic model yields

$$\chi^{-1}(\theta)=\frac{1-[3+b^2(1-2\beta\delta)]\theta^2-b^2(2\beta\delta-3)\theta^4}{1-[b^2(1-2\beta)-3c]\theta^2-b^2c(3-2\beta)\theta^4}.$$

When $b^2=3(3-2\beta)^{-1}$ and $c=(2\beta\delta-3)(3-2\beta)^{-1}$, this expression reduces to unity.

[33]J. A. White and B. S. Maccabee, Phys. Rev. Lett. 27, 223 (1971). The values for β and γ found in the present investigation (Table III) lead to $\eta\geq 0.09=\alpha$. If $\eta=\alpha$, then $\nu=(\gamma/d)^{1/2}$, provided (Refs. 28 and 29) $2-\alpha=\nu d$. Here $d=3$ is the dimensionality of the system. Values found for β and γ in the present investigation (Table III) lead to $\nu=0.637$.

[34]B. S. Maccabee and J. A. White, Bull. Am. Phys. Soc. 19, 603 (1974).

[35]G. Gouy, C. R. Acad. Sci. (Paris) 115, 720 (1892).